**Ken Gall**
**Jiankuai Diao**
**Martin L. Dunn**

Department of Mechanical Engineering, University of Colorado at Boulder, Boulder, CO 80309

**Michael Haftel**
**Noam Bernstein**
**Michael J. Mehl**

Center for Computational Materials Science, Naval Research Laboratory, Washington, DC 20375-5345

# Tetragonal Phase Transformation in Gold Nanowires

*First principle, tight binding, and semi-empirical embedded atom calculations are used to investigate a tetragonal phase transformation in gold nanowires. As wire diameter is decreased, tight binding and modified embedded atom simulations predict a surface-stress-induced phase transformation from a face-centered-cubic (fcc) ⟨100⟩ nanowire into a body-centered-tetragonal (bct) nanowire. In bulk gold, all theoretical approaches predict a local energy minimum at the bct phase, but tight binding and first principle calculations predict elastic instability of the bulk bct phase. The predicted existence of the stable bct phase in the nanowires is thus attributed to constraint from surface stresses. The results demonstrate that surface stresses are theoretically capable of inducing phase transformation and subsequent phase stability in nanometer scale metallic wires under appropriate conditions.* [DOI: 10.1115/1.1924558]

## 1 Introduction

Gold (Au) nanowires have potential application in nanotechnology due to their relative ease of fabrication [1,2], stability at small scales [3–13], capacity for biomolecule functionalization [14–17], and high conductivity. Recent studies have demonstrated that low-dimension Au materials can exist in non-face centered cubic (fcc) structures. When thinned below a critical size, ⟨110⟩ Au nanowires have been observed to transform into a helical multi-shell structure [10]. Small ⟨100⟩ Au nanowires are predicted to undergo an fcc to body centered cubic (bct) phase transformation [18]. Atoms in single chain Au nanowires have different spacing than atoms along close-packed directions in bulk Au [12]. The formation of non-fcc crystal structures in Au nanowires is driven by surface stresses and the tendency to minimize surface energy. In order to fully exploit Au nanowires in emerging nanosystems, it is critical to understand their unique structures from a fundamental perspective. In addition, the study of phase stability and transformation in nanometer scale solids has broad implications. From a basic science point of view, the study of phase changes in nanometer scale materials provides fundamental information on solid-state transformations not easily ascertained in bulk solids [19,20]. From an application standpoint, control of metastable phases in nanometer scale materials may provide a means for small-scale actuation, analogous to martensitic transformations observed in nanoscale biological systems [21,22].

Nanometer scale solids possess unique properties due in part to their large ratio of surface area to volume. Free surfaces in solids give rise to surface energy and surface stress. Surface stresses, which are typically tensile in metals, cause contraction of surface atoms relative to bulk atoms, resulting in "intrinsic" compressive stresses within materials. Intrinsic stresses are defined as stresses existing in a material in the absence of external applied load. Although free surfaces exist in macroscopic materials, surface-stress-induced intrinsic compressive stresses are significant only in materials with nanometer scale dimensions. The surface-stress-induced intrinsic compressive stress state depends on sample geometry. Figure 1 is a schematic illustrating the effect of *tensile* surface stress on the development of intrinsic *compressive* stresses in the core of freestanding nanometer scale materials. The core of a nanometer scale solid is defined as the remainder of the material excluding the first few atomic surface layers. A nanofilm is defined by one dimension being nanometer scale, a boundary condition that creates intrinsic in-plane biaxial compression in the film core. Nanowires possess nanometer scales in two dimensions, and a resulting intrinsic stress state of triaxial compression in the wire core. Nanoparticles have nanometer scales in all three dimensions, and thus an intrinsic stress state of hydrostatic compression in the particle core. The intrinsic stress states depicted in Fig. 1 are ideal, since cross-sectional shape and exposed surface orientation can alter the resulting stress state. The magnitude of the intrinsic stresses in nanometer scale materials increases with decreasing sample size in the nanometer scale dimension. Moreover, the intrinsic stresses in nanofilms or nanoparticles can be *proportionately* modified by experimental methods: forced epitaxial growth for nanofilms [23,24] and application of hydrostatic pressure for nanoparticles [19,20]. On the other hand, the unique triaxial stress state in nanowires (hydrostatic pressure plus uniaxial compression) is more difficult to uniformly adjust.

The intrinsic stresses in nanowires can result in a tetragonal crystal lattice distortion [23–27], which can drive the formation of a bct lattice from a host fcc lattice. Theoretical predictions have revealed a local minimum energy bct phase formed by tetragonal distortion of the fcc lattice [23,27]. However, the predicted bct structure is typically elastically unstable with respect to shear [23,27], thus requiring stabilization by "external" forces. In this sense, the bct structure is not a classical metastable phase, as defined for bulk materials. Although prior work has considered stabilization of the bct structure by epitaxial film growth [23,24], it may be possible to stabilize an elastically unstable phase in a freestanding material by surface stresses [18]. The objective of the present paper is to explore the stability of tetragonal states in freestanding fcc Au nanowires using various theoretical approaches. The present work provides a stronger theoretical foundation for initial semi-empirical atomistic predictions of the fcc to bct phase transformation in Au nanowires [18].

## 2 Simulation Methods

Simulations were performed using the embedded atom method (EAM) [28], the modified embedded atom method (MEAM) [29], the tight binding (TB) [30] method, and density functional theory

Contributed by the Materials Division of ASME for publication in the JOURNAL OF ENGINEERING MATERIALS AND TECHNOLOGY. Manuscript received September 21, 2004. Final manuscript received December 28, 2004. Review conducted by: Min Zhou.

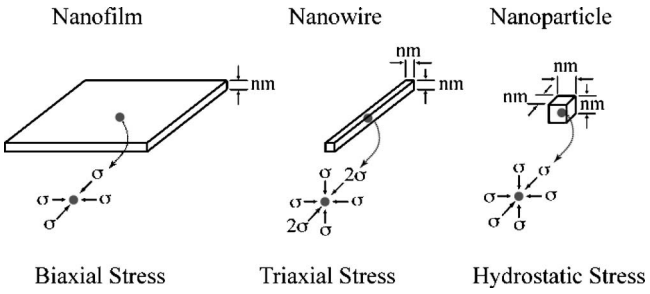


**Fig. 1 Schematic of three different freestanding nanometer scale materials. Tensile surface stresses result in unique intrinsic compressive stress states in the material cores. The nanofilm experiences an in-plane biaxial stress, the nanowire experiences a triaxial stress state, with a larger component along the wire axis, and the nanoparticle experiences a hydrostatic stress state.**

(DFT) using the Vienna ab initio simulation package (VASP) [31]. Complete details regarding the various methods are found in respective Refs. [28–31]. Briefly, EAM and MEAM are semiempirical approaches that use a pair-potential term and an embedding energy term to implicitly capture some electronic structure *effects*. The EAM potentials are parametrized to the sublimation energy, equilibrium fcc lattice constant, elastic constants, and vacancy formation energy [28], while the MEAM potentials are fit to the sublimation energy, equilibrium fcc lattice constant, elastic constants, vacancy formation energy, and two structural energy differences relative to fcc (bcc and hcp) [29]. In addition, the electron density in the EAM potential is given by the superposition of spherically averaged atomic electron density, while MEAM potential use angularly dependence electron density to account for the angular dependence of bonding. The TB method bases energy calculations on a set of reduced electronic degrees of freedom. The free TB parameters are fit to band structure and total energies, typically of the bulk fcc and bcc phases, determined from first principles calculations [30]. Compared to EAM and MEAM, the TB method typically offers improved predictive capacity at the expense of maximum atomic domain size. The DFT method we employ involves a pseudopotential, and the local density approximation, and results in the precise evaluation of the electronic ground state of atomic systems at finite temperature [31]. The local density approximation typically overestimates cohesive energies, but provides a good description of energy differences based on first principles. We implement our DFT calculations with the VASP code [31] using ultrasoft pseudopotentials. Simulation predictions are also compared to existing first-principle calculations when possible. MEAM simulations were performed on a nonperiodic wire with a 32 nm length, TB simulations were performed on a periodic wire in the length direction with two atomic layers, and first principle calculations were performed with full periodicity (simulating the bulk). We note that wire length and periodicity can influence the wire transformation, however, this effect is not examined here.

## 3 Results and Discussion

Calculated surface stresses, $f_{ij}$, for Au are presented in Table 1. Simulations were performed on atomic slabs using published techniques [32,33]. Previous DFT [34–37] results are included for reference. In solids, surface stress is not equivalent to surface energy, $\gamma$, but is defined as the strain derivative of the surface energy:

$$f_{ij} = [\partial(A\gamma)/\partial\varepsilon_{ij}]/A = \gamma\delta_{ij} + \partial\gamma/\partial\varepsilon_{ij}, \quad i,j = 1,2 \qquad (1)$$

where $A$ is the surface area, $\gamma$ is the surface energy, and $\varepsilon_{ij}$ is the elastic strain in the plane of the surface. In liquids, the surface energy is equal to the surface stress in magnitude, since atoms are free to migrate to and from the surface and mitigate changes in the surface energy with strain (e.g., the second term in Eq. (1) is zero). The surface stress is a second-rank tensor with four components and units of force per unit length. The surface stress is isotropic for {100} and {111} surfaces and anisotropic on the {110} surface (Table 1). The EAM and MEAM predictions underestimate the surface stress magnitude relative to DFT, while the EAM, MEAM, and TB predictions demonstrate reverse ordering of surface stress for {111} and {100} surfaces, relative to DFT. In contrast to predictions from other methods, MEAM predicts a negative (compressive) surface stress in the ⟨100⟩ direction for a {110} surface. The relative surface stress magnitudes in Table 1 are important since they control the driving force for a stress-induced phase transformation in a nanowire.

**Table 1 Surface stresses in fcc gold for various surface orientations and in-plane directions. Calculations were performed using methods defined in the main text.**

| Surface (i) | Direction (j) | Surface Stress, $f_{ij}$ (J/m$^2$) | | | |
|---|---|---|---|---|---|
| | | EAM | MEAM | TB | DFT[34-37] |
| {100} | Isotropic | 1.57 | 1.03 | 3.64 | 4.57[34], 4.60[35] |
| {111} | Isotropic | 1.76 | 1.47 | 4.82 | 2.77[36], 2.56[37] |
| {011} | <100> | 0.89 | -0.37 | 2.42 | -- |
| | $<0\bar{1}1>$ | 1.54 | 1.12 | 4.09 | -- |

The surface stresses in Table 1 quantify the driving force for a possible surface stress-induced phase transformation in nanowires. However, to achieve an fcc to bct transformation, the intrinsic stress state in the wire (Fig. 1) must coincide with the Bain path for the transformation. This coordination occurs when the wire axis is ⟨100⟩. The exposed side surfaces are determined by wire cross-section shape and relative rotation around the wire axis with respect to the base cubic system. For a square cross-section, no rotation would yield [010] and [001] side surfaces, while a 45° rotation would provide [011] and [0-11] surfaces. The significance of the negative surface stress predicted by MEAM, in the ⟨100⟩ direction on the {110} surface, is now apparent. A wire with a [100] axis and [010], [001] side surface experiences the stress state depicted in Fig. 1, for all calculation methods in Table 1. This stress state leads to net compression along the wire axis, driving wire contraction along the Bain path. A wire with a [100] axis and [011] and [0-11] side surfaces also experiences the stress state depicted in Fig. 1 when constrained by surface stresses predicted by EAM and TB. On the other hand, the negative surface stress value in MEAM causes expansion of a ⟨100⟩ wire (with ⟨110⟩ side surfaces) along the Bain path, resulting in a stress state differing from triaxial compression. The predicted expansion is in the opposite direction as required for an fcc to bct transformation, as will be demonstrated in bulk Au simulations. In the present work, the simulated nanowires only have {100} side surfaces, and for the {100} surfaces, all methods predict positive surface stresses, and TB and DFT predict comparable surface stress magnitudes (Table 1).

Figure 2 is a plot of energy as a function of lattice spacing for bulk (periodic) Au deformed along a ⟨100⟩ orientation. The energy values in Fig. 2 are provided with respect to the predicted energies of the unstrained fcc structure using respective methods. The agreement between the various calculation methods is reasonable. All predictions show a global minimum at the fcc structure and a local minimum at a bct structure caused by compression of the fcc lattice. The lattice parameters and the cohesive energies of the

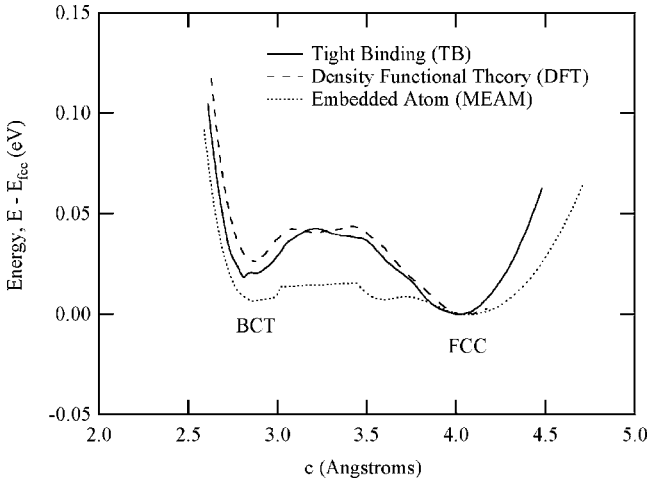


**Fig. 2 Energy as a function of lattice spacing for various simulation methods. The curves were generated by displacement-controlled expansion and contraction of bulk periodic Au along the [100] fcc axis. The [010] and [001] axes were allowed to adjust freely. Energy minimums exist for fcc and bct phases.**

predicted bct structures are listed in Table 2. The EAM potentials did not predict a low energy bct phase, while the MEAM potential predicts two low energy bct phases [18], evident from the two energy wells left of the fcc well (Fig. 2). MEAM also predicts the lowest energy barrier to formation of the bct phase compared to TB and DFT. All three methods produce somewhat wavy curves during the energy peak in the range of c=3.5 to 3.0 Å. The prediction of the second bct phase by MEAM (Table 2) is noteworthy since the potentials were not fit to a bct structure and MEAM only implicitly accounts for electronic degrees of freedom in calculations. Based on the results in Fig. 2, the bct phase can be induced by compression of a fcc lattice along the ⟨100⟩ axis. The stress state in the ⟨100⟩ nanowires is thus capable of facilitating the fcc to bct transformation since it consists of uniaxial compression with superimposed hydrostatic stress (Fig. 1). For all methods, the uniaxial intrinsic stress required to induce the phase change from fcc to bct is on the order of 4 GPa, a value attainable in nanometer scale wires given the surface stress magnitudes in Table 1.

Although the various theoretical formulations predict the same energy minimum for the bct phase in bulk Au, and surface stresses can generate the stresses required to induce this phase, it is necessary to examine the elastic stability of the bulk bct phase. Table 3 summarizes the elastic constants of the bulk bct phase predicted by the various calculation methods. A tetragonal structure is elastically unstable if the shear constant $(C_{11}-C_{12})/2$ is less than zero [23,27]. From Table 3, MEAM predicts that the bct phase is elastically stable while TB and DFT predict elastic instability in the bct phase. The elastic stability predicted by MEAM implies a metastable bulk bct phase, while the bulk bct phase in DFT and TB simulations is classically unstable.

Molecular static and dynamic simulations were performed on nanowires with TB, EAM, and MEAM methods. Nanowire simulations using the various methods all confirm that a ⟨100⟩ wire, with {100} side surfaces, experiences intrinsic compression along its ⟨100⟩ axis as depicted in Fig. 1. The magnitude of intrinsic compressive stress in a nanowire depends on the simulation model, the exposed side surface orientations, and scales proportionately with $f/d$, where $f$ is the surface stress magnitude and $d$ is the wire diameter. As wire diameter is decreased, the increasing intrinsic compressive stress drives increased elastic contraction of nanowires (with respect to a bulk fcc lattice) upon static energy minimization (relaxation). Below a critical wire size, both TB and MEAM simulations predict that an fcc ⟨100⟩ Au nanowire will transform into a bct Au nanowire. The EAM simulations predict that small ⟨100⟩ wires will not transform into a bct structure, but rather reorient through slip into a low energy fcc ⟨110⟩ nanowire [38]. MEAM simulations also predict reorientation of a ⟨100⟩ wire into a ⟨110⟩ wire above the critical wire size, where the transformation to the final bct structure is less energetically favorable [38].

Figure 3 presents a three-dimensional view of (a) an original ⟨100⟩ fcc wire and (b) the minimum energy ⟨100⟩ bct wire predicted by TB. The wire contracts approximately 30% in the length direction and expands in the transverse direction, consistent with MEAM predictions [18]. Figure 4 presents the relaxed atomic positions for transformed bct wires calculated using (*a*) TB and (*b*) MEAM. The wires in Fig. 4 began as 1.63 by 1.63 nm ⟨100⟩ fcc wires, which were relaxed to a minimum energy state by the conjugate gradient method. The cross section of the wire shown in Fig. 4(*a*) is from the wire shown in Fig. 3(*b*). In Fig. 4, two adjacent ⟨100⟩ planes are shown, and the dashed box highlights the bct lattice, which differs only slightly between the two methods. The lattice parameters of the nanowire bct phases predicted

**Table 2 Lattice parameters and cohesive energy for the Au bct phase. Calculations were performed using methods defined in the main text.**

| Parameter | EAM | MEAM | TB | DFT | DFT[27] |
|---|---|---|---|---|---|
| a (Angstroms) | Unstable | 3.404 | 3.466 | 3.423 | -- |
| c (Angstroms) | | 2.856 | 2.810 | 2.859 | -- |
| c/a | | 0.839 | 0.811 | 0.835 | 0.852 |
| $E_{bct}$ - $E_{fcc}$ (eV) | | 0.006 | 0.019 | 0.018 | 0.021 |
| $E_{bct}$ (eV) | | -3.924 | -3.848 | -4.375 | -- |

**Table 3 Elastic constants for the Au bct phase. Calculations were performed using methods defined in the main text.**

| Elastic Constant Term | Elastic Constant Value (GPa) | | |
|---|---|---|---|
| | MEAM | TB | DFT[27] |
| $C_{11}$ | 151.5 | 181.3 | -- |
| $C_{12}$ | 131.0 | 187.1 | -- |
| $C_{13}$ | 145.1 | 190.7 | -- |
| $C_{33}$ | 243.6 | 244.5 | -- |
| $C_{44}$ | 6.2 | 49.9 | -- |
| $C_{66}$ | 15.2 | 81.2 | 177 |
| $C' = (C_{11} - C_{12})/2$ | 10.3 | -2.9 | -40 |

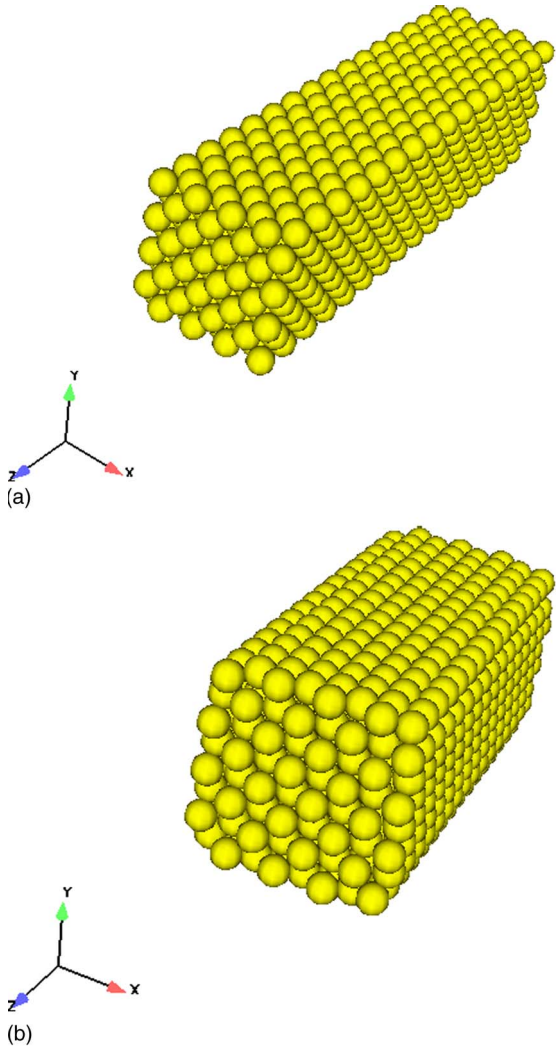


**Fig. 3 Three-dimensional image of a nanowire (*a*) before (fcc) and (*b*) after (bct) transformation predicted by static TB energy minimization simulations**

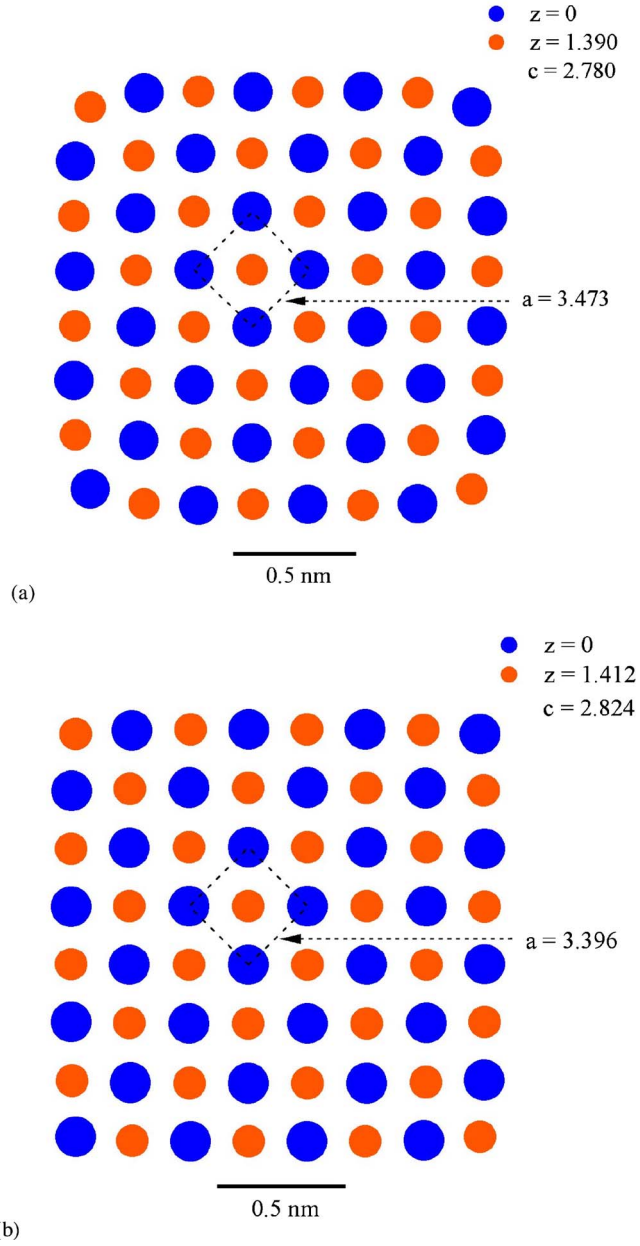


**Fig. 4 Cross-section view of two parallel atomic planes from a bct nanowire predicted by (*a*) TB simulations and (*b*) MEAM simulations. Both wires began as ⟨100⟩ fcc wires with a size of 1.63 by 1.63 nm and were relaxed to the lower energy bct state. The orientation of the bct wire is [100] with [011] and [0-11] side surfaces.**

by both methods are consistent with the bulk bct phase predictions in Table 2, with relative expansion in "*a*" and contraction in "*c*" due to surface stresses in the bct wire. The {100} side surfaces of the original fcc wire are now ⟨110⟩ bct surfaces. Aside from slight differences in the atomic positions near the edges and free surfaces, the bct nanowire structure predicted by TB and MEAM in Fig. 4 are basically identical.

The TB and DFT simulations both predict that the bct phase observed in the nanowire (Fig. 4) is unstable in the bulk with respect to shear. Consequently, the low temperature stability of the bct phase in the nanowires simulated by TB is caused by the surface stresses in the new bct nanowire. Simulated annealing of the nanowires in a molecular dynamics framework was performed using TB and MEAM. The MEAM wire retained its precise structure during simulated annealing. The TB wire maintained a bct structure, although the surfaces became irregular. We also note that the small periodic length (two atomic layers) in the TB simulation is restrictive since it may prevent dislocation nucleation, which may preclude the transformation. Further work is needed to examine the effects of temperature and possible dislocation activity on nanowire transformation and stability. The intrinsic stresses induced by the surface stresses act in a manner analogous to epitaxial mismatch strains in thin film growth, since they stabilize a phase that would not be observed in the bulk [23,24]. The stabilizing mechanism in the epitaxial films is due to the fixed strain constraint from the substrate, not due to surface stresses, although the epitaxial strain constraint does cause intrinsic stress in the film.

The phase transformation occurs when the work from the intrinsic compressive stress in the wire is large enough to overcome the barrier to the formation of the higher energy bct phase. Since the intrinsic compressive stress in the wire increases with a decrease in wire diameter, a critical wire diameter exits for the stress-induced phase transformation. The predicted critical wire size is a function of the transformation driving force (the surface

stress magnitude Table 1) and the resistance to the transformation (the work required to overcome the energy barrier to form the bct phase in Fig. 2). The TB, DFT, and MEAM calculations all predict a similar critical stress to the formation of the bct phase, approximately 4 GPa, calculated by the maximum slope of the energy curve left of the fcc well in Fig. 2 (leftmost well for MEAM). From the fcc state, the surface-stress-induced driving force for the transformation is higher in TB and DFT calculations (Table 1). However, the MEAM simulations predict an intermediate bct phase with higher surface stresses and consequently a larger driving force for the transformation. Under the assumption of pure compressive loading, the critical wire size, $d_{crit}$, for transformation is given as

$$d_{crit} = 4f/\sigma_{crit} \tag{2}$$

where $f$ is the surface stress magnitude, and $\sigma_{crit}$ is the critical stress required for the fcc to bct transformation. For the TB simulations, $f = 3.64\ J/m^2$ and $\sigma_{crit} = 4$ GPa, resulting in $d_{crit} = 3.64$ nm. The wire simulated in Figs. 3 and 4 had an original size of $d = 1.63$, below the $d_{crit}$ value. Larger wire sizes were not examined due to limitations in the maximum system size with TB. We note that the superimposed hydrostatic stress on the nanowires (Fig. 1) inhibits the transformation since it restricts lateral expansion, effectively decreasing the critical wire diameter necessary to achieve the transformation. However, the transformation ultimately occurs due to the proportionately large compressive component in the triaxial stress state. The method for calculating the critical wire size for the MEAM simulations is the same except it is necessary to use parameters for both bct phase transformations. Prior MEAM work [18,32] has shown a smaller critical wire diameter (2.56 nm) owing to the smaller surface stresses predicted by MEAM relative to TB. Based on the present TB and first-principles simulations, the intermediate bct phase transformation predicted by MEAM is artificial.

## 4 Conclusions

In summary, surface stresses in fcc Au nanowires can lead to tetragonal distortions and a theoretical stress-induced fcc to bct phase transformation. The results demonstrate that the surface-stress-induced intrinsic stresses in nanowires can result in phase stability analogous to that caused by epitaxial growth of nanometer scale thin films. More accurate TB and first-principles calculations confirm the existence the phase transformation and the final bct structure predicted using semi-empirical MEAM simulations [18]. However, TB and first-principle calculations predict a larger surface-stress-induced transformation driving force and no intermediate bct phase, relative to MEAM predictions. To achieve the transformation, the surface-stress-induced triaxial stress in the wire core must coincide with a Bain path for the fcc to bct transformation, which occurs for ⟨100⟩ nanowires. Further work is needed to examine nanowire stability as a function of temperature. From an experimental perspective, the phase transformation will not be observed in wires produced by "bottom-up" fabrication methods [1,2], since these wires typically grow in low-energy fcc configurations with ⟨110⟩ orientations. However, material removal approaches in "top-down" nanowire fabrication methods [6,10], can potentially be used to explore fcc wires with ⟨100⟩ initial orientations and the theoretical fcc to bct transformation.

## Acknowledgments

The work of KG, JD, and MLD is supported by Sandia National Laboratories, NSF, and DOE. The work of MH, NB, and MM was supported by ONR. Computer programs developed under the Department of Defense CHSSI program of the High Perfomance Computation Modernization Project (HCMCP) were utilized as well as the VASP code available at its facilities.

## References

[1] Johnson, C. J., Dujardin, E., Davis, S. A., Murphy, C. J., and Mann, S., 2002, "Growth and Form of Gold Nanorods Prepared by Seed-Mediated, Surfactant-Directed Synthesis," J. Mater. Chem., **12**, pp. 1765–1770.
[2] Xia, Y., Yang, P., Sun, Y., Wu, Y., Mayers, B., Gates, B., Yin, Y., Kim, F., and Yan, H., 2003, "One-Dimensional Nanostructures: Synthesis, Characterization, and Applications," Adv. Mater. (Weinheim, Ger.), **15**, pp. 353–389.
[3] Agrait, N., Rubio, G., and Vieira, S., 1995, "Plastic Deformation of Nanometer-Scale Gold Connective Necks," Phys. Rev. Lett., **74**, pp. 3995–3998.
[4] Brandbyge, M., Schiotz, J., Sorensen, M. R., Stoltze, P., Jacobsen, K. W., Norskov, J. K., Olesen, L., Laegsgaard, E., Stensgaard, I., and Besebbacher, F., 1995, "Quantized Conductance in Atom-Sized Wires Between Two Metals," Phys. Rev. B, **52**, pp. 8499–8514.
[5] Stalder, A., and Durig, U., 1996, "Study of Plastic Flow in Ultrasmall Au Contacts," J. Vac. Sci. Technol. B, **14**, pp. 1259–1263.
[6] Kondo, Y., and Takayanagi, K., 1997, "Gold Nanobridge Stabilized by Surface Structure," Phys. Rev. Lett., **79**, pp. 3455–3458.
[7] Ohnishi, H., Kondo, Y., and Takayanagi, K., 1998, "Quantized Conductance Through Individual Rows of Suspended Gold Atoms," Nature (London), **395**, pp. 780–783.
[8] Yanson, A. I., Bollinger, G. R., van der Brom, H. E., Agrait, N., and Ruitenbeek, J. M., 1998, "Formation and Manipulation of a Metallic Wire of Single Gold Atoms," Nature (London), **395**, pp. 783–785.
[9] Marszalek, P. E., Greenleaf, W. J., Li, H., Oberhauser, A. F., and Fernandez, J. M., 2000, "Atomic Force Microscopy Captures Quantized Plastic Deformation in Gold Nanowires," Proc. Natl. Acad. Sci. U.S.A., **97**, pp. 6282–6286.
[10] Kondo, Y., and Takayanagi, K., 2000, "Synthesis and Characterization Of Helical Multi-Shell Gold Nanowires," Science, **289**, pp. 606–608.
[11] Rodrigues, V., Fuhrer, T., and Ugarte, D., 2000, "Signature of Atomic Structure in Quantum Conductance of Gold Nanowires," Phys. Rev. Lett., **85**, pp. 4124–4127.
[12] Rodrigues, V., and Ugarte, D., 2001, "Real-Time Imaging of Atomistic Process in One-Atom Thick Metal Junctions," Phys. Rev. B, **63**, p. 073405.
[13] Wang, B., Yin, S., Wang, G., Buldum, A., and Zhao, J., 2001, "Novel Structures and Properties of Gold Nanowires," Phys. Rev. Lett., **86**, pp. 2046–2049.
[14] Zhong, Z. Y., Male, K. B., and Luong, J. H. T., 2003, "More Recent Progress in the Preparation of Au Nanostructures, Properties, and Applications," Anal. Lett., **36**(15), pp. 3097–3118.
[15] Wagner, P., Hegner, M., Kernen, P., Zaugg, F., and Semenza, G., 1996, "Covalent Immobilization of Native Biomolecules Onto Au(111) Via N-Hydroxysuccinimide Ester Functionalized Self-Assembled Monolayers for Scanning Probe Microscopy," Biophys. J., **70**(5), pp. 2052–2066.
[16] Rabkeclemmer, C. E., Leavitt, A. J., and Beebe, T. P., 1994, "Analysis of Functionalized DNA Absorption on Au(111) Using Electron-Spectroscopy," Langmuir, **10**(6), pp. 1796–1800.
[17] Savran, C. A., Knudsen, S. M., Ellington, A. D., and Manalis, S. R., 2004, "Micromechanical Detection of Proteins Using Aptamer-Based Receptor Molecules," Anal. Chem., **76**(11), pp. 3194–3198.
[18] Diao, J., Gall, K., and Dunn, M., 2003, "Surface Stress Induced Phase Transformation in Metal Nanowires," Nat. Mater., **2**, pp. 656–660.
[19] Jacobs, K., Zaziski, D., Scher, E. C., Herhold, A. B., and Alivisatos, A. P., 2001, "Activation Volumes for Solid-Solid Transformation in Nanocrystals," Science, **293**, pp. 1803–1806.
[20] Zaziski, D., Prilliman, S., Scher, E. C., Casula, M., Wickham, J., Clark, S. M., and Alivisatos, A. P., 2004, "Critical Size for Fracture During Solid–Solid Phase Transformations," Nano Lett., **4**, pp. 943–946.
[21] Olson, G. B., and Hartman, H., 1982, "Martensite and Life—Displacive Transformations as Biological Processes," J. Phys. (France), **43**, pp. 855–865.
[22] Kanamaru, S., Leiman, P. G., Kostyuchenko, V. A., Chipman, P. R., Mesyanzhinov, V. V., Arisaka, F., and Rossmann, M. G., 2002, "Structure of the Cell-Puncturing Device of Bacteriophage T4," Nature (London), **415**, pp. 553–557.
[23] Jona, F., and Marcus, P. M., 2002, "Tetragonal States of Palladium I. Theory," Phys. Rev. B, **65**, p. 155403.
[24] Ji, X. Z., Tian, Y., and Jona, F., 2002, "Tetragonal States of Palladium II. Experiment," Phys. Rev. B, **65**, p. 155404.
[25] Wills, J. M., Eriksson, O., Soderlind, P., and Boring, A. M., 1992, "Trends in the Elastic Constants of Cubic Metals," Phys. Rev. Lett., **68**, pp. 2802–2805.
[26] Mehl, M. J., and Boyer, L. L., 1991, "Calculation of Energy Barriers for Physically Allowed Lattice-Invariant Strains in Aluminum and Iridium," Phys. Rev. B, **43**, pp. 9498–9502.
[27] Mehl, M. J., Aguayo, A., Boyer, L. L., and de Coss, R., 2004, "Absence of Metastable States in Strained Monatomic Cubic Crystals," Phys. Rev. B, **70**, p. 014105.
[28] Daw, M. S., and Baskes, M. I., 1984, "Embedded-Atom Method: Derivation and Application to Impurities, Surfaces, and Other Defects in Metals," Phys. Rev. B, **29**(12), 6443.
[29] Baskes, M. I., 1992, "Modified Embedded-Atom Potentials for Cubic Materials And Impurities," Phys. Rev. B, **46**, pp. 2727–2742.
[30] Mehl, M. J., and Papaconstantopoulos, D. A., 1996, "Applications of a Tight-Binding Total-Energy Method for Transition and Noble Metals: Elastic Constants, Vacancies, and Surfaces of Monatomic Metals," Phys. Rev. B, **54**(7), pp. 4519–4530.
[31] Kresse, G., and Furthmüller, J., 1996, "Efficient Iterative Schemes for Ab Initio Total-Energy Calculations Using a Plane-Wave Basis Set," Phys. Rev. B,

**54**, p. 11169.
[32] Diao, J., Gall, K., and Dunn, M. L., 2004, "Atomistic Simulation of the Structure and Elastic Properties of Metal Nanowires," J. Mech. Phys. Solids, **52**(9), pp. 1935–1962.
[33] Streitz, F. H., Cammarata, R. C., and Sieradzki, K., 1994, "Surface-Stress Effects on Elastic Properties. I. Thin Metal Films," Phys. Rev. B, **49**(15), pp. 10699–10706.
[34] Fiorentini, V., Methfessel, M., and Scheffler, M., 1993, "Reconstruction Mechanism of fcc Transition Metal (001) Surfaces," Phys. Rev. Lett., **71**(7), pp. 1051–1054.
[35] Yu, B. D., and Scheffler, M., 1997, "Physical Origin of Exchange Diffusion on fcc(100) Metal Surfaces," Phys. Rev. B, **56**(24), pp. R15569–R15572.
[36] Needs, R. J., Godfrey, M. J., and Mansfield, M., 1991, "Theory of Surface Stress and Surface Reconstruction," Surf. Sci., **242**(1), pp. 215–221.
[37] Kollar, J., Vitos, L., Osorio-Guillen, J. M., and Ahuja, R., 2003, "Calculation of Surface Stress for fcc Transition Metals," Phys. Rev. B, **68**(24), p. 245417.
[38] Diao, J., Gall, K., and Dunn, M. L., 2004, "Surface Stress Driven Reorientation of Gold Nanowires," Phys. Rev. B, **70**, p. 075413.